January, 2015

Model for electronic transport properties of thermoelectric semiconductor materials

BSc. Thesis

Aswin Witte

Supervisors:

Prof. dr. ir. B.J. Geurts

Dr. ir. M. Huijben

UNIVERSITY OF TWENTE.

Contents

1 Introduction **3**

2 Theory **6**

2.1 Seebeck effect 6

2.2 Doped semiconductors 6

2.3 Band structure 6

3 Model **9**

3.1 Density of states 10

3.2 Energy distribution function 10

3.3 Scattering mechanisms 10

3.3.1 Ionized impurity scattering 11

3.3.2 Phonon scattering 11

3.3.3 Piezoelectric scattering 12

3.3.4 Grain interfaces 12

3.4 Fermi level 13

3.5 Summary of the model 14

4 Implementation **15**

4.1 Indefinite integrals 15

4.2 Tolerance 15

4.3 Units 16

5 Results and Discussion **18**

5.1 Verification and validation 18

5.2 Tolerance 19

5.3 Tuning 20

5.3.1 Deformation potential 20

5.3.2 Band gap 22

5.4 Impurities 23

5.5 Metallic behaviour 24

6 Conclusions and Recommendations **25**

7 Acknowledgements **26**

Appendices **27**

A Matlab code **27**
A.1 Model.m 27
A.2 PbTe.m 28
A.3 Emaxalt.m 29
A.4 Fermidirac.m 30
A.5 Difffermi.m 30
A.6 Scattering1.m 31
A.7 Scattering2.m 32
A.8 Dofs.m 33

1 Introduction

In view of global energy and environmental issues, the necessity to utilize our energy resources more efficiently becomes relevant. Since most energy is still being discharged into the environment as waste heat, significant amounts of renewable energy remains unused. Thermoelectric power generation systems offer a feasible method to convert available heat energy directly into electrical energy, irrespective of source size. However, implementation of present-day semiconductor materials into practical thermoelectric applications has been hampered due to toxic and/or scarce elements and poor chemical stability at high temperatures. The use of silicide compounds as promising thermoelectric materials has enormous potential to overcome the above-mentioned problems, if their thermal conductivity can be reduced. In this report we formulate a model with which the thermal and electrical conductivity of such materials can be predicted. We also show some first results obtained with this approach, which holds a promise toward application in more detailed design of new materials for energy.
Figure 1 shows a schematic overview of a thermoelectric power generator. The efficiency of a generator depends not just on the power produced, but also on how much heat is provided at the hot junction. As a thermoelectric generator is a heat engine, its efficiency is limited by the Carnot efficiency, the fundamental limit on the thermal efficiency due to the second law of thermodynamics. The Carnot efficiency is given by [1]:

$$\eta_{Carnot} = 1 - \frac{T_C}{T_H} \tag{1}$$

where T_H is the temperature at the hot junction and T_C the temperature at the cold junction.

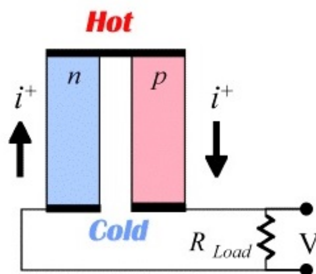

Figure 1: A schematic overview of a thermoelectric generator. [1]

The efficiency of a thermoelectric generator is further limited by the thermoelectric properties, Seebeck coefficient, electrical resistivity and thermal conductivity. These material properties all appear together and form a new material property called the

Thermoelectric figure of merit, Z. The maximum efficiency of a thermoelectric device is given by [1]:

$$\eta = \frac{T_H - T_C}{T_H} \frac{\sqrt{1 + ZT} - 1}{\sqrt{1 + ZT} + \frac{T_C}{T_H}} \tag{2}$$

where Z the figure of merit and T the average temperature (given by $\frac{T_H + T_C}{2}$).

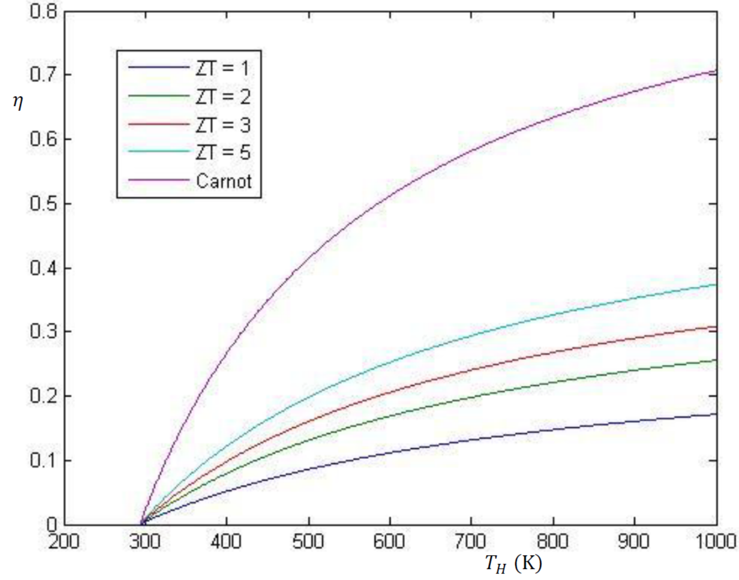

Figure 2: The maximum efficiency of a thermoelectric device as function of the temperature at the hot junction. The temperature at the cold junction is fixed at 293 K and the efficiency is shown for several values of the figure merit as well for the Carnot efficiency.

As shown in Figure 2, the higher the figure of merit of a material, the more efficient the material is at converting heat to electricity. A figure of merit of 3 is necessary for succesful implementation, though nowadays research reaches a figure of merit of about 1. In this figure T_C is set to room temperature (293 K) and the efficiency is shown as a function of the temperature at the hot junction for a number of values of the dimensionless figure of merit (ZT). The figure of merit of a material and the dimensionless figure of merit are defined as [2]:

$$Z = \frac{\sigma S^2}{\kappa_e + \kappa_p} \tag{3}$$

$$ZT = \frac{\sigma S^2}{\kappa_e + \kappa_p} T \tag{4}$$

where σ is the electrical conductivity, S is the Seebeck coefficient, κ_e is the electronic thermal conductivity and κ_p is the lattice thermal conductivity.

The goal is to come as close as possible to the Carnot efficiency and therefore to maximize the dimensionless figure of merit. In material properties this means a high electrical conductivity, a high Seebeck coefficient and a low thermal conductivity. Realistic expressions for the individual quantities defining ZT can help us finding ways to improve this material properties.

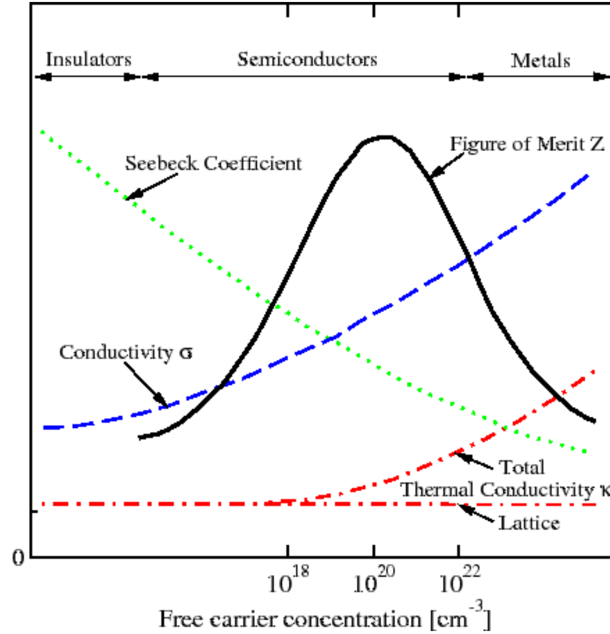

Figure 3: The dependence of the Seebeck coefficient, electrical conductivity, thermal conductivity and figure of merit on the free carrier concentration. [3]

As a first step materials can be divided into insulators, semiconductors and metals, depending on the free carrier concentration of the material. All three parameters defining the figure of merit depend on this free carrier concentration, Figure 3 shows this dependence for the Seebeck coefficient, electrical conductivity and thermal conductivity as well for the figure of merit. From this figure one can see that the figure of merit reaches a maximum in the region of heavily doped semiconductors. Consequently, this will be the type of material of interest to adapt in order to further increase the figure of merit. In this report we model an isotropic material consisting of multiple crystallites. The area where crystallites meet are known as grain boundaries.
The report is organized as follows. The theory is presented in section 2. In section 3 the model is discussed followed by the implementation of the model in section 4. In section 5 the results of the model are presented in comparison to experimental values for PbTe. The conclusions and recommendations are given in section 6.

2 Theory

The physical phenomenon behind thermoelectric materials is called the thermoelectric effect. The thermoelectric effect is the direct conversion of a temperature difference to an electric voltage and vice versa. The term thermoelectric effect is a collective noun for the Seebeck effect, Peltier effect and Thomson effect. As we are interested in energy generation the Seebeck effect is of interest in this report.

2.1 Seebeck effect

The Seebeck effect is the conversion of temperature differences directly into electricity. It is caused by the diffusion of charge carriers in metals or semiconductors. Charge carriers on the hot side of the material have higher fluctuations than charge carriers on the cold side of the material. This results in diffusion of carriers to the cold side. The increased carrier concentration on the cold side causes an electric field which counteracts the diffusion force. The strength of the effect can be decribed by the Seebeck coefficient:

$$S = -\frac{\Delta V}{\Delta T} \tag{5}$$

where ΔV is the potential difference generated by the temperature difference ΔT. The sign of S depends on whether electrons (n-type) or holes (p-type) are the majority charge carriers.

2.2 Doped semiconductors

A doped or extrinsic semiconductor is an intrinsic (pure) semiconductor with added impurities. Impurity atoms are atoms of a different element than the atoms of the intrinsic semiconductor and can act as either donor or acceptor.
Donor impurity atoms have more valence electrons than the atom they replace, providing excess electrons to the intrinsic semiconductor. This increases the electron carrier concentration of the semiconductor, making it n-type.
Acceptor impurity atoms have fewer valence electrons than the atom they replace, providing excess holes to the intrinsic semiconductor. This increases the hole carrier concentration of the semiconductor, making it p-type.

2.3 Band structure

The electronic band structure of a solid describes the ranges of energy that an electron within the solid may have (bands) and the ranges of energy it may not have (band

gaps). There are infinitely many of these bands and band gaps, but a material has a limited amount of electrons to fill the bands. The band with the highest energy in which electrons are normally present at absolute zero temperature is called the valence band (see Figure 4a). The band right above the valence band is called the conduction band. In semiconductors there is a small band gap between the valence band and the conduction band. This means that at temperatures close to absolute zero there is no electrical conduction possible. When energy is applied to semiconductors (in the form of heat) individual electrons can move from the valence band to the conduction band. This electron can move freely within the conduction band. As a result of the jump of this electron a hole is formed in the conduction band, which can move freely within this band as well. The electron and hole together are called a charge carrier pair and contribute to the electrical conductivity.

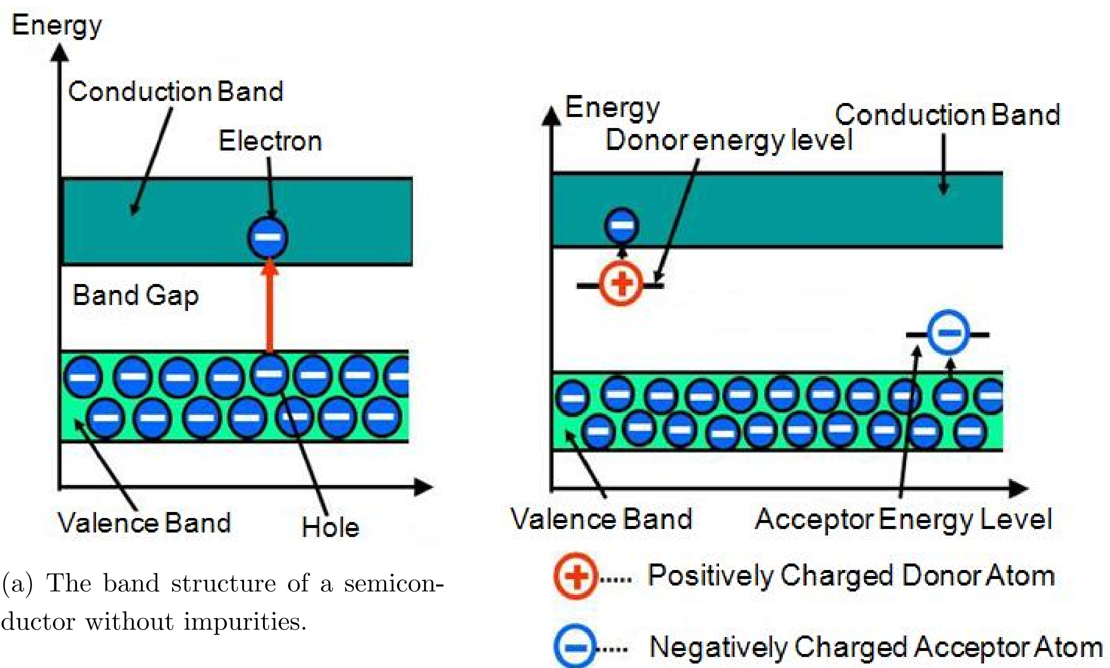

(a) The band structure of a semiconductor without impurities.

(b) The changes in band structure when adding donor or acceptor impurities.

Figure 4: The band structure of a semiconductor and the changes due to adding donor or acceptor impurities to the semiconductor. [4]

Doping causes a change in this structure, as shown in Figure 4b. By using donor impurities an energy level is created in the band gap close to the conduction band. An electron

from the donor level can be elevated to the conduction band very easily. Similarly, by using acceptor impurities an energy level is created close to the valence band. An electron from the valence band can move into the acceptor energy level again very easily. In this way, the electrical properties are influenced by the concentration of dopants.

3 Model

The model presented in this paper is on approaching the solution of the Boltzmann equation on the basis of a relaxation time approximation. The essence of this approach is the assumption that scattering processes can be described by a relaxation time τ that specifies how the distribution function f approaches its equilibrium f_0. The Boltzmann equation is given by: [5]

$$\frac{\partial f}{\partial t} + v \cdot \nabla_r f - \frac{e\epsilon}{\hbar} \cdot \nabla_k f = \left(\frac{\partial f}{\partial t}\right)_{coll} \tag{6}$$

where $f(r, k, t)$ is the distribution function, r is a point in the crystal, k is the Bloch wave vector of an electron [5] and the collision term on the right-hand side contains all the information about the nature of the scattering. Another assumption is that we consider an isotropic thermoelectric material, which means that the electrical conductivity, Seebeck coefficient and other values are direction independent. [2] [5] Furthermore we suppose the motion of carriers is in quasi-equilibrium and that the charge carriers are scattered in such a way that their relaxation time, τ, may be expressed in terms of energy by the relation $\tau = \tau_0 E^r$, where τ_0 and r are constants.
Then by solving the Boltzmann equation one finds the resulting formulas for the electrical conductivity, σ, the Seebeck coefficient, S and the electronic thermal conductivity, κ_e [5]: (The upper sign (+) of S refers to n-type semiconductors and the lower sign (-) to p-type)

$$\sigma = -\frac{2e^2}{3m^*} \int_0^\infty g(E)\tau(E)E\frac{\partial f_0(E)}{\partial E}\mathrm{d}E \tag{7}$$

$$S = \pm\frac{1}{eT}\left[\mu - \frac{\int_0^\infty g(E)\tau(E)E^2\frac{\partial f_0(E)}{\partial E}\mathrm{d}E}{\int_0^\infty g(E)\tau(E)E\frac{\partial f_0(E)}{\partial E}\mathrm{d}E}\right] \tag{8}$$

$$\kappa_e = \frac{2}{3m^*T}\left[\frac{\left(\int_0^\infty g(E)\tau(E)E^2\frac{\partial f_0(E)}{\partial E}\mathrm{d}E\right)^2}{\int_0^\infty g(E)\tau(E)E\frac{\partial f_0(E)}{\partial E}\mathrm{d}E} - \int_0^\infty g(E)\tau(E)E^3\frac{\partial f_0(E)}{\partial E}\mathrm{d}E\right] \tag{9}$$

where e is the electron charge, m^* is the effective mass, μ is the Fermi level, $g(E)$ is the density of states, $\tau(E)$ is the relaxation time for the charge carriers and $f_0(E)$ is the energy distribution function.
$g(E)$, $\tau(E)$ and $f_0(E)$ are energy E dependent functions and also depend on several other material specific physical parameters. These functions will be introduced and motivated individually below.

3.1 Density of states

The model assumes that the electronic structure inside the grain formations is the same as the electronic structure of the bulk material, thus the grain boundary (interface between the bulk thermoelectric material and the nanostructure inclusions) does not affect significantly the energy-band structure and it serves only as a scattering interface.

It has been shown that the Kane model is a good description for the energy dispersion of small band-gap semiconductors: [2] [6]

$$\frac{\hbar^2 k_l^2}{2m_l^*} + \frac{\hbar^2 k_t^2}{2m_t^*} = E + \alpha E^2 \tag{10}$$

where $\hbar$ is Planck's constant, $k_{l,t}$ is the carrier momentum and $m_{l,t}^*$ the effective mass along the longitudinal and transverse direction. $\alpha = \frac{1}{E_g}$ is a nonparabolicity factor, where E_g is the band-gap. As a result the total density of states, $g(E)$, can be written as:

$$g(E) = \frac{\sqrt{2}}{\pi^2} \left(\frac{m^*}{\hbar^2}\right)^{\frac{3}{2}} \sqrt{E\left(1 + \frac{E}{E_g}\right)} \left(1 + 2\frac{E}{E_g}\right) \tag{11}$$

where the effective mass is defined as $m^* = \beta^{2/3} \left(m_l^* m_t^{*2}\right)^{1/3}$. The band-gap, E_g, is temperature dependant: $E_g = E_g^0 + \gamma T$ where E_g^0 is the band-gap at $T = 0$ K and γ is a material specific parameter.

3.2 Energy distribution function

The free electron theory of electron conduction in solids considers each electron as moving in a periodic potential produced by the ions and other electrons without disturbance. Then it regards the deviation from periodicity due to vibrations of the lattice as a perturbation. The distribution function that measures the number of electrons at energy E is called $f(E)$. In equilibrium this is given by the Fermi-Dirac distribution: [5]

$$f_0(E) = \frac{1}{\exp\left(\frac{E-\mu}{k_b T}\right) + 1} \tag{12}$$

where μ is the Fermi level and k_b is the Boltzmann constant.

3.3 Scattering mechanisms

For the relaxation time, $\tau(E)$, there are contributions from different scattering mechanisms. We assume that these individual scattering mechanisms can be associated with

a resistivity, hence we can apply Mathiessen's rule to obtain the total relaxation time:

$$\frac{1}{\tau(E)} = \sum_i \frac{1}{\tau_i(E)} \tag{13}$$

where τ_i is the contribution from each separate mechanism.
Below several mechanisms will be described with an explanation whether to include this mechanisms in our model or not.

3.3.1 Ionized impurity scattering

We are looking at semiconductors which are heavily doped. This doped semiconductor can be a p-type, containing an excess of holes, or n-type, containing an excess of electrons. Both ways these donors and/or acceptors are typically ionized and thus charged. This causes an electron or hole approaching the ionized impurity to deflect due to Coulombic forces. This is known as ionized impurity scattering. The amount of deflection is modelled by: [2]

$$\tau_{imp}(E) = \left(\frac{Z^2 e^4 N_i}{16\pi\sqrt{2m^*}\epsilon^2} \ln\left[1 + \left(\frac{2E}{E_m}\right)^2\right]\right)^{-1} E^{\frac{3}{2}} \tag{14}$$

where Z is the number of charges per impurity, e is the electron charge, N_i is the concentration of ionized impurities, m^* is the effective mass, ϵ is the dielectric constant of the medium and $E_m = \frac{Ze^2}{4\pi\epsilon r_m}$ is the potential energy at a distance r_m from an ionized impurity. r_m is approximately half the mean distance between two adjacent impurities. This form of scattering is only relevant when there is a significant concentration of ionized impurities.

3.3.2 Phonon scattering

Considering a temperature above absolute zero, vibrating atoms create pressure waves, or phonons. Phonons can be considered to be particles and they can interact with electrons and holes and scatter them. At higher temperatures there will be more phonons, thus increasing the phonon scattering.
Acoustic phonons are coherent movements of atoms of the lattice out of their equilibrium positions and the amount of deflection by this type of phonons is modelled by: [2]

$$\tau_{a-ph}(E) = \frac{h^4}{8\pi^3} \frac{\rho v_L^2}{k_b T} \frac{1}{(2m^*)^{\frac{3}{2}} D^2} E^{-\frac{1}{2}} \tag{15}$$

Optical phonons are out-of-phase movement of the atoms of the lattice and the amount of deflection by this type of phonons is modelled by: [2]

$$\tau_{o-ph}(E) = \frac{h^2}{\sqrt{2m^* e^2 k_b T \left(\epsilon_\infty^{-1} - \epsilon_0^{-1}\right)}} E^{\frac{1}{2}} \tag{16}$$

3.3.3 Piezoelectric scattering

A piezoelectric effect can occur in compound semiconductors, semiconductors which consist of element from two of more different groups of the periodic table. This may lead to local electric fields that deflect the carriers. The effect of piezoelectric scattering is small in most semiconductors and in only important at low temperatures, when other scattering mechanisms are weaker. As we not yet that interested in temperatures close to the absolute zero, this mechanism is left out of this model for now.

3.3.4 Grain interfaces

The grain regions in the material are assumed to have the same average characteristics. Then the grain interfaces can be modelled as rectangular potential barriers with average height E_b, width w, and distance between them L.
When carriers with energy E encounter such a barrier, the transmission probability for the charge carriers through a single barrier is $T(E)$. The path length of a carrier that has passed the first barrier and is scattered by the second is given by $T(E)(1-T(E))L$. The mean-free path after scattering from the Nth barrier becomes: [2]

$$\lambda = \sum_{n=1}^{\infty} T(E)^n \left(1 - T(E)\right) nL = \frac{T(E)L}{1 - T(E)} \tag{17}$$

Assuming that there are an infinite number of barriers, the summation can be expressed as shown in Eq. (17). Then the relaxation time due to this type of scattering is given by

$$\tau_b(E) = \frac{\lambda}{v} \tag{18}$$

where $v = \sqrt{\frac{2E}{m^*}}$, the average velocity of the carriers. The expression for the transmission probability through a single barrier can be obtained following quantum-mechanical considerations. [7] For the separate regions when the carrier energy is smaller or larger

than the barrier height, one finds:

$$\tau_b(E) = \begin{cases} L\sqrt{\frac{m^*}{2E}} \left[1 + \frac{4\frac{E}{E_b}\left(1-\frac{E}{E_b}\right)}{\sinh^2\left[\sqrt{\frac{2m^* E_b w^2}{\hbar^2}\left(1-\frac{E}{E_b}\right)}\right]} \right] & \text{if } E < E_b \\ L\sqrt{\frac{m^*}{2E}} \left[1 + \frac{4\frac{E}{E_b}\left(\frac{E}{E_b}-1\right)}{\sin^2\left[\sqrt{\frac{2m^* E_b w^2}{\hbar^2}\left(\frac{E}{E_b}-1\right)}\right]} \right] & \text{if } E > E_b \end{cases} \tag{19}$$

3.4 Fermi level

The Fermi-Dirac distribution given in (12) contains an important parameter, the Fermi level. This parameter is specific for each material and is related to the charge-carrier concentration p via:

$$p = \frac{4}{\sqrt{\pi}} \left(\frac{2\pi m^* k_b T}{h^2} \right)^{3/2} \int_0^\infty \left(\frac{E}{k_b T} \right)^{1/2} f_0(E) \mathrm{d}\frac{E}{k_b T} \tag{20}$$

where μ is hidden in $f_0(E)$ as shown earlier:

$$f_0(E) = \frac{1}{\exp\left(\frac{E-\mu}{k_b T}\right) + 1}$$

One can determine the Fermi level μ for a specific concentration p by solving the above equation. This can be done by a root finding algorithm.

3.5 Summary of the model

To summarize this chapter a list of all relevant formulas for the model is given:

$$Z = \frac{\sigma S^2}{\kappa_e + \kappa_p} \tag{21}$$

$$\sigma = -\frac{2e^2}{3m^*}\int_0^\infty g(E)\tau(E)E\frac{\partial f_0(E)}{\partial E}\mathrm{d}E \tag{22}$$

$$S = \pm\frac{1}{eT}\left[\mu - \frac{\int_0^\infty g(E)\tau(E)E^2\frac{\partial f_0(E)}{\partial E}\mathrm{d}E}{\int_0^\infty g(E)\tau(E)E\frac{\partial f_0(E)}{\partial E}\mathrm{d}E}\right] \tag{23}$$

$$\kappa_e = \frac{2}{3m^*T}\left[\frac{\left(\int_0^\infty g(E)\tau(E)E^2\frac{\partial f_0(E)}{\partial E}\mathrm{d}E\right)^2}{\int_0^\infty g(E)\tau(E)E\frac{\partial f_0(E)}{\partial E}\mathrm{d}E} - \int_0^\infty g(E)\tau(E)E^3\frac{\partial f_0(E)}{\partial E}\mathrm{d}E\right] \tag{24}$$

$$g(E) = \frac{\sqrt{2}}{\pi^2}\left(\frac{m^*}{\hbar^2}\right)^{\frac{3}{2}}\sqrt{E\left(1+\frac{E}{E_g}\right)}\left(1+2\frac{E}{E_g}\right) \tag{25}$$

$$f_0(E) = \frac{1}{\exp\left(\frac{E-\mu}{k_bT}\right)+1} \tag{26}$$

$$\frac{1}{\tau(E)} = \sum_i \frac{1}{\tau_i(E)} \tag{27}$$

$$\tau_{imp}(E) = \left(\frac{Z^2e^4N_i}{16\pi\sqrt{2m^*}\epsilon^2}\ln\left[1+\left(\frac{2E}{E_m}\right)^2\right]\right)^{-1}E^{\frac{3}{2}} \tag{28}$$

$$\tau_{a-ph}(E) = \frac{h^4}{8\pi^3}\frac{\rho v_L^2}{k_bT}\frac{1}{(2m^*)^{\frac{3}{2}}D^2}E^{-\frac{1}{2}} \tag{29}$$

$$\tau_{o-ph}(E) = \frac{h^2}{\sqrt{2m^*}e^2k_bT\left(\epsilon_\infty^{-1}-\epsilon_0^{-1}\right)}E^{\frac{1}{2}} \tag{30}$$

$$\tau_b(E) = \begin{cases} L\sqrt{\frac{m^*}{2E}}\left[1+\frac{4\frac{E}{E_b}\left(1-\frac{E}{E_b}\right)}{\sinh^2\left[\sqrt{\frac{2m^*E_bw^2}{\hbar^2}\left(1-\frac{E}{E_b}\right)}\right]}\right] & \text{if } E < E_b \\ L\sqrt{\frac{m^*}{2E}}\left[1+\frac{4\frac{E}{E_b}\left(\frac{E}{E_b}-1\right)}{\sin^2\left[\sqrt{\frac{2m^*E_bw^2}{\hbar^2}\left(\frac{E}{E_b}-1\right)}\right]}\right] & \text{if } E > E_b \end{cases} \tag{31}$$

$$p = \frac{4}{\sqrt{\pi}}\left(\frac{2\pi m^*k_bT}{h^2}\right)^{3/2}\int_0^\infty\left(\frac{E}{k_bT}\right)^{1/2}f_0(E)\mathrm{d}\frac{E}{k_bT} \tag{32}$$

4 Implementation

The model decribed in section 3 was written in Matlab. The code is contained in Appendix A. In this section the complications in implementing the model are discussed.

4.1 Indefinite integrals

As shown in the model section, the integrals needed to evaluate the electrical conductivity, Seebeck coefficient and thermal conductivity are indefinite, extending to infinite energy. However, at high energies the term $\frac{\partial f_0(E)}{\partial E}$ rapidly goes to zero. As shown in Figures 5a, 5b and 5c, this will dominate the integrand. Thus the high energy levels hardly contribute to the final value of the integral. Now the question remains what cutoff energy is appropriate. The answer is that the relevant energies highly depend on the temperature and the Fermi level of the material, so a fixed boundary will not work. As shown in Figures 5a and 5d, a higher temperature will cause a lower and broader peak, so the cutoff energy should be higher at higher temperatures. To implement this, two different options were evaluated; a multiple of the energy at which the integrand is maximal and a multiple of the Fermi level. What these figures also show is that the energy at which the integrand is maximum increases with increasing temperature, thus a boundary which is a multiple of this E_{max} is a good choice. The boundary has been varied from E_{max} up to 100 times E_{max}. The results were indistinguishable from 6 times the point of maximal integrand. To be safe the boundary has been set on 10 times E_{max} as shown in Appendix A. E_{max} is found by computing the integrand at an array of energies and using Matlab's max command.

4.2 Tolerance

In the report of Lars Corbijn van Willenswaard [8] he stated that a fixed absolute integration precision, as used by Matlab's quad, will result in bad accuracy. However, when manually entering an integration precision and tolerance the result did not change. One could conclude that Matlab's absolute integration precision is small enough not to cause any problems for our model. It was also stated that a solution to the bad accuracy in integrating is to integrate over the dimensionless energy, $\frac{E}{k_b T}$, instead of E. In papers this is quite common, but not motivated. When implementing this dimensionless energy the difference in the integral value was abolished by the change in the pre-factor, making this an unnecessary adaptation.

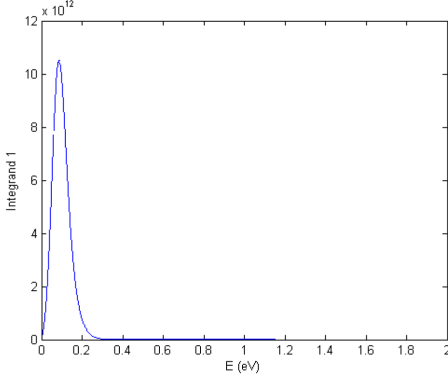

(a) A plot of the first integrand, or $-g(E)\tau(E)E\frac{\partial f_0(E)}{\partial E}$, versus energy at 300 K.

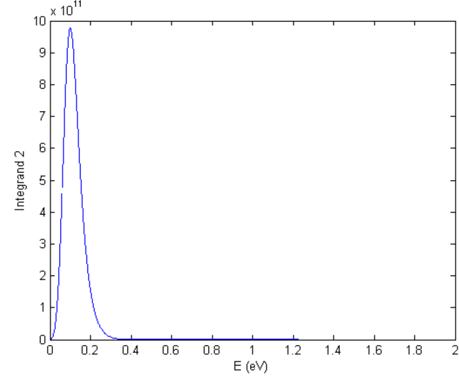

(b) A plot of the second integrand, or $-g(E)\tau(E)E^2\frac{\partial f_0(E)}{\partial E}$, versus energy at 300 K.

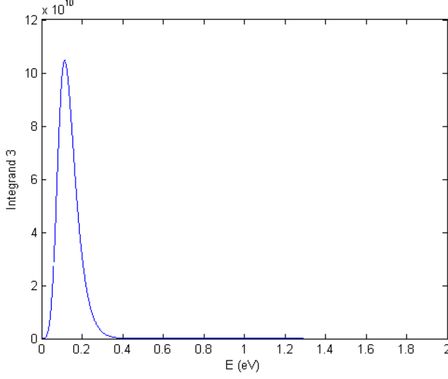

(c) A plot of the third integrand, or $-g(E)\tau(E)E^3\frac{\partial f_0(E)}{\partial E}$, versus energy at 300 K.

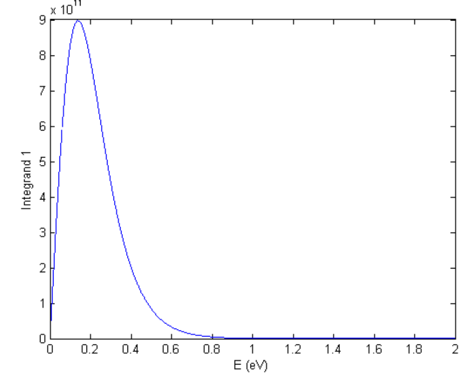

(d) A plot of the first integrand, or $-g(E)\tau(E)E\frac{\partial f_0(E)}{\partial E}$, versus energy at 1000 K.

Figure 5: Plots of the different integrand necessary to evaluate the electrical conductivity, Seeback coefficient and thermal conductivity. The parameters used are those of PbTe.

4.3 Units

To get some sort of control, the model presented in the previous chapter is a copy of the model presented by Popescu et al. [2] A good first check is a unit test. This test was performed with a peculiar result. In the expression of the charge-carrier concentration, p, which is used to determine the Fermi level, the units don't match if one assumes the energy, E, has Joule as unit which is consistent with the rest of the paper. To clarify, the formula mentioned by Popescu is:

$$p = \frac{4}{\sqrt{\pi}}\left(\frac{2\pi m^* k_b T}{h^2}\right)^{3/2}\int_0^\infty E^{1/2} f(E)\mathrm{d}E \tag{33}$$

When the energy, E, is taken to be unitless, the problem is solved. To avoid misinterpretations the equation is modified to (20):

$$p = \frac{4}{\sqrt{\pi}} \left(\frac{2\pi m^* k_b T}{h^2} \right)^{3/2} \int_0^\infty \left(\frac{E}{k_b T} \right)^{1/2} f_0(E) \mathrm{d} \frac{E}{k_b T}$$

Thereby it is taken into account that $f_0(E)$ already is a unitless expression. Besides, there are some small differences between the formulas presented in section 3.5 and the Matlab code from Appendix A. At some points, a factor e^a, with a a rational number, is added to the Matlab code. This is to compensate for the fact that all energies in Matlab are implemented in electron volts instead of Joules. This is done because the amount of energy involved is small making it more clear to present these amounts in electron volts.

5 Results and Discussion

5.1 Verification and validation

Before experimenting with inclusions and changing parameters the model needs to be verified. The model from section 3 comes from the paper of A. Popescu et al. [2] and a good first step in verification is to compare the found results with the results published in the paper.
When parameters as mentioned in the article are used, the result is shown in Figure 6.

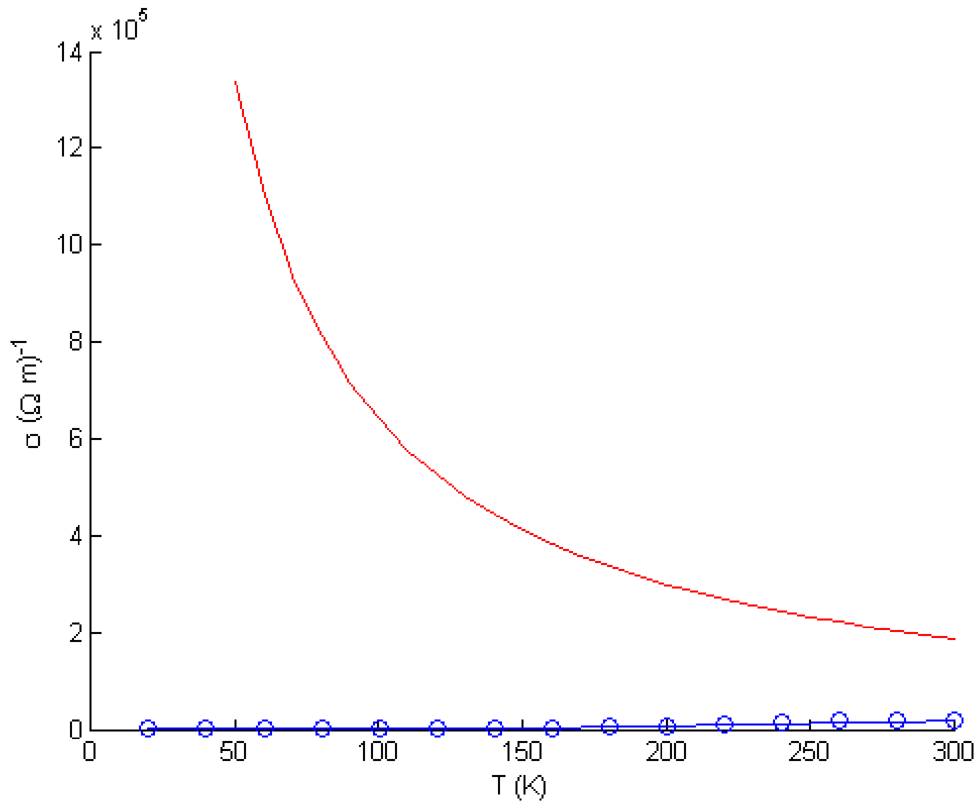

Figure 6: The electrical conductivity versus the absolute temperature. The blue open circles represent the experimentally obtained data point given in the paper, the blue line represents the theoretical model by A. Popescu et al. and the red line represents the model described in this paper.

The parameters used are: $E_b = 60$ meV, $w = 50$ nm, $L = 300$ nm, $m^* = 0.16 \cdot m_0$, where m_0 is the mass of an electron, $\rho = 8160$ kg/m^3, $v_L = 1730$ m/s, $\epsilon_\infty^{-1} - \epsilon_0^{-1} = 0.0072 \cdot E_g$, $D = 10$ eV and $E_g = 0.19 + 0.0004 \cdot T$.

As shown there is a big difference between the results found by Popescu and my results, where the experimental data point support Popescua, especially at low temperatures where the two models diverge. With the same parameters the plot in Figure 7 of Seeback coefficient versus temperature is made. Here the results have the same trend, though at a temperature of 300 K this model is 100% off compared to the experimental data.

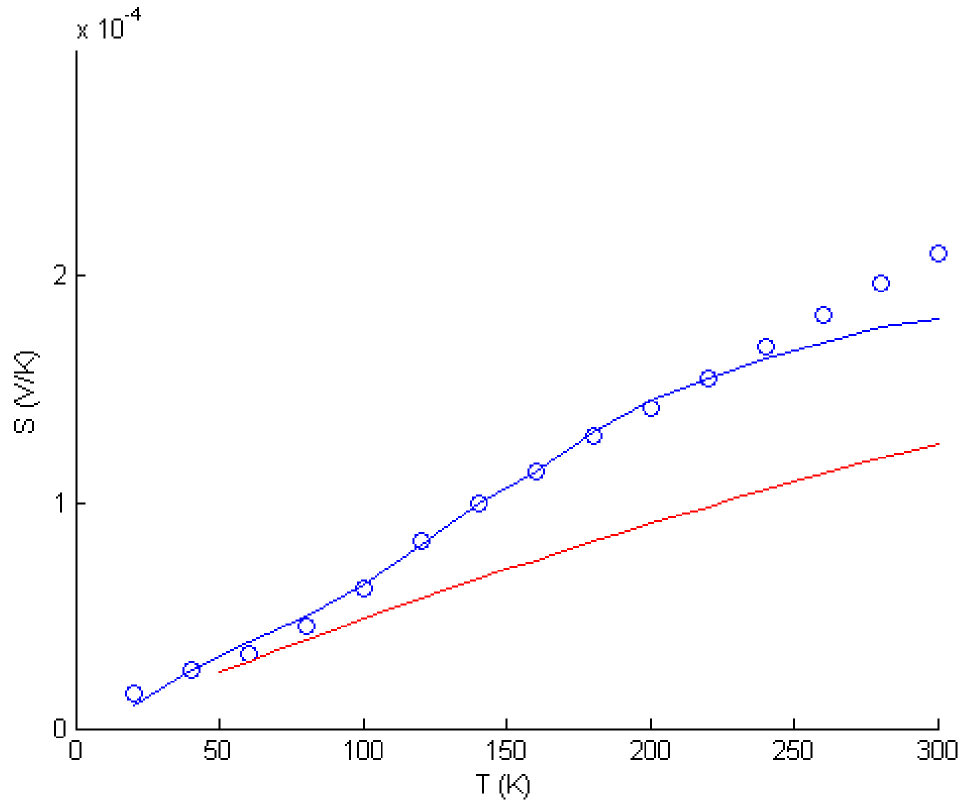

Figure 7: The Seeback coefficient versus the absolute temperature. The blue open circles represent the experimentally obtained data point given in the paper, the blue line represents the theoretical model by A. Popescu et al. and the red line represents the model described in this paper.

5.2 Tolerance

From Figure 6 it is clear that a whole other trend is found for the electrical conductivity at low temperatures. This might have to do with the absolute tolerance of the integral that needs to be computed for σ at low temperatures, see (22). To check this, the electrical conductivity is calculated for different tolerances at a temperature of 50 K.

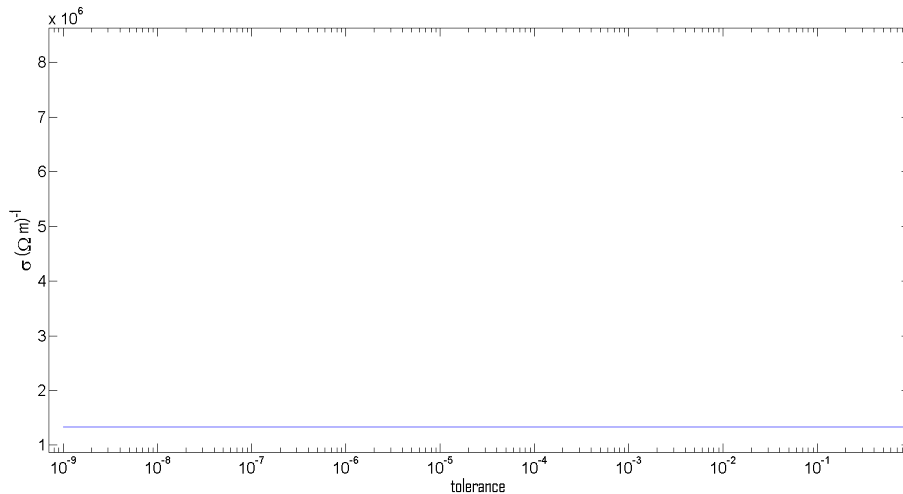

Figure 8: The electrical conductivity versus the absolute tolerance at $T = 50$ K

The result is shown in Figure 8 and is a horizontal line, so the absolute tolerance does not influence the value of the electrical conductivity.

5.3 Tuning

As the models in section 3 and Appendix A match and the results do not, something is incorrect. As the formulas the models consist off are also seen in other reports about transport properties of thermoelectric semiconductors with different purposes, it is not likely these are wrong. The parameters are harder to verify, because they are very material specific. In an attempt to match the results one could tune some of the variables. Obviously there is a difference in dependence of the electrical conductivity on temperature, especially for low temperatures. Therefore parameters like γ, D, etcetera, which directly influence the temperature dependence seem to be a good first guess.

5.3.1 Deformation potential

In the paper of Popescu et al. it is mentioned that the value of D is varied in the range of 5 - 15 eV. In the results shown above this deformation potential is taken to be 10 eV. In Figures 9a and 9b the results for a deformation potential of respectively 5 and 15 eV.

A higher deformation potential is lowering the value of the electrical conductivity, bringing it closer to the experimental results presented by Popescu et al. but is not changing the trend. This is shown clearly by entering a deformation potential of 100 eV, which is shown in Figure 10.

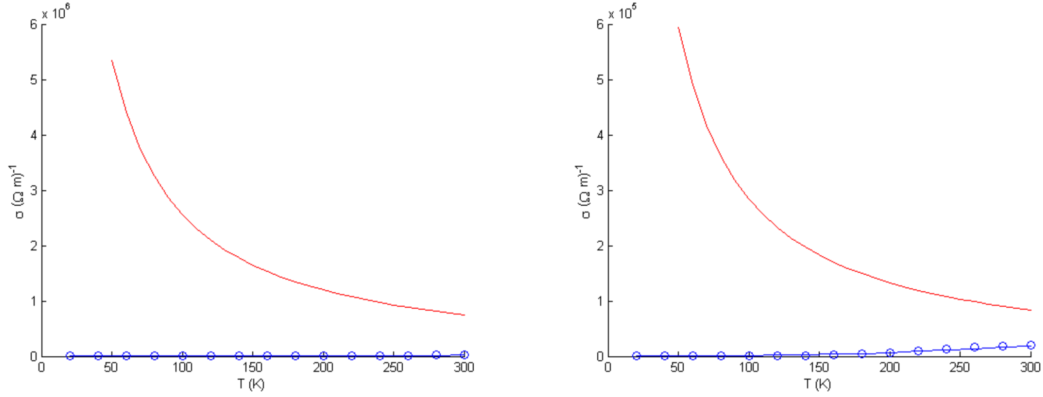

(a) The electrical conductivity versus the absolute temperature. The red line represents the model described in this paper with a deformation potential of 5 eV.

(b) The electrical conductivity versus the absolute temperature. The red line represents the model described in this paper with a deformation potential of 15 eV.

Figure 9: The electrical conductivity versus temperature for two different deformation potentials.

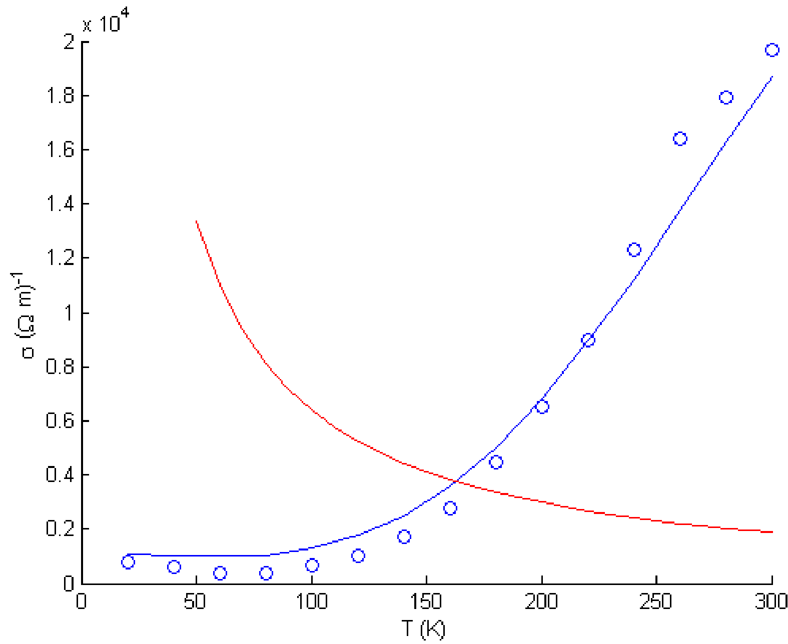

Figure 10: The electrical conductivity versus the absolute temperature. The red line represents the model described in this paper with a deformation potential of 100 eV.

5.3.2 Band gap

Other parameters as the effective mass, longitudinal velocity of sound, mass density and dielectric constants are preceding temperature in the same way as the deformation potential, so altering them would not change the trend either. The only other option in changing parameters is γ, the temperature dependence of the band gap. Where this parameter is stated to be positive, a negative relation between band gap and temperature could explain the trend difference in the plot of electrical conductivity versus temperature. In Figure 11 the electrical conductivity is plotted versus temperature with $\gamma = -0.0004$ eV/K. The deformation potential is left at 100 eV to make the change more clear to see. A small change is visible for temperatures from 200 to 300 K, but the trend remains the same.

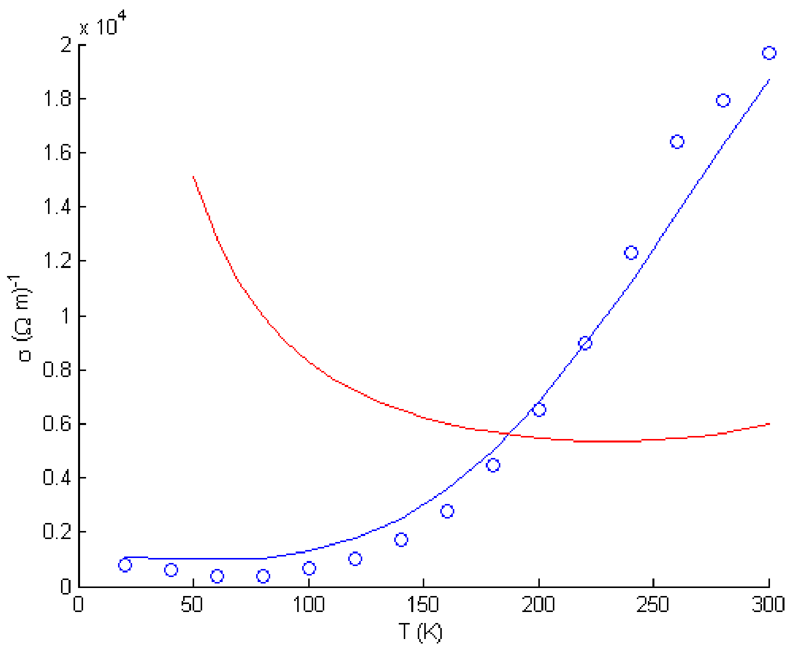

Figure 11: The electrical conductivity versus the absolute temperature. The red line represents the model described in this paper with $\gamma = -0.0004$ eV/K and $D = 100$ eV.

Subsequently, the question remains whether these mathematical adaptations make sense physically. In work done by L.G. Ferreira [9], quite some time ago, the deformation potential of Lead Telluride is analized extensively. The conclusion of his work states that the exact value of the deformation potential cannot be determined and the range of values of 5 to 15 eV mentioned in the work of Popescu et al. is confirmed. A negative gradient

in a band gap versus temperature plot is usual in most semiconductors, however not with tellurides. So the mathematical adaptations have minimal to no influence and they are not supported by the physics.

5.4 Impurities

When presenting their results, Popescu et al. mention that since the synthesized and measured samples did not contain a significant concentration of ionized impurities, the ionized impurity scattering mechanism in not taken into account. Consequently, in the results shown in Figures 6 to 11 this scattering mechanism was neglected. To make sure this was an accurate assumption this scattering mechanism should be included and results should not differ. In Figure 12 the result is shown when ionized impurity scattering is included. The parameters used are: $Z = 2$ (Ag^{2+} as impurities), $N_i = 0.15p$ as Popescu et al. use later in their report, $\epsilon = 1000$ and $r_m = 1$ nm. The result is as expected inseparable from Figure 6.

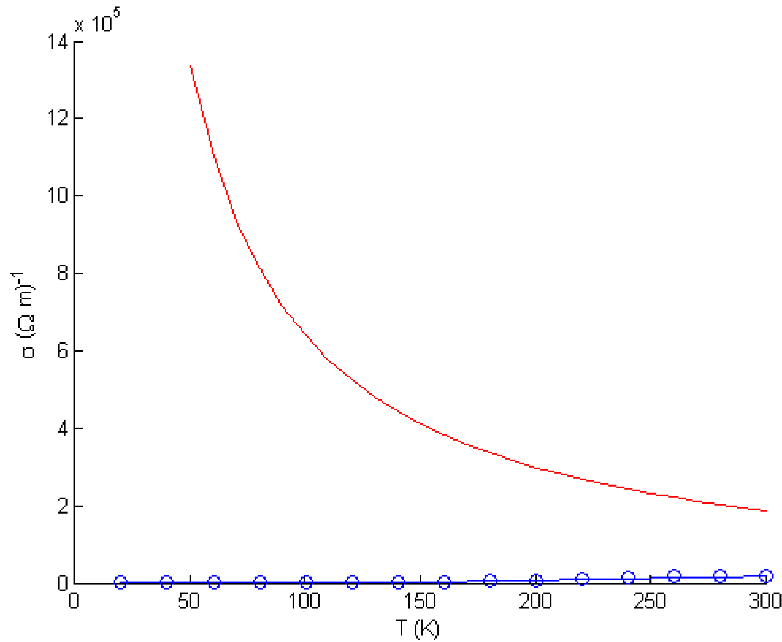

Figure 12: The electrical conductivity versus the absolute temperature with the ionized impurity scattering mechanism taken into account.

Also tuning N_i and r_m to respectively $0.5p$ and 0.1 nm does not affect the result notably.

5.5 Metallic behaviour

In the previous subsection different changes have been presented to try to change the behaviour of the electrical conductivity at low temperatures, without succes. Remarkably the behaviour shown is metallic, a higher electrical conductivity at lower temperatures. This could indicate that some parameters used represent a metal instead of the semiconductor we try to model. Research into which parameters represent metals and ought to be change to resemble a semiconductor should lead to verification of the results presented by Popescu et al.

6 Conclusions and Recommendations

In this report a model has been presented to calculate the electrical conductivity, Seebeck coefficient and electronic thermal conductivity of a semiconductor material with or without impurities. This could be of great use to predict the thermoelectric figure of merit of a material. Subsequently, one might be able to find the optimal material parameters for the best possible thermoelectric material, by means of tuning parameters as the concentration of impurities.

When trying to reach these optimistic goals, one of the first steps caused a huge bump in the road to success. To be more concrete, an attempt to reproduce results published by Popescu et al. failed. One could come up with several reason for this failure, one of which is the inability of the writer of this report to properly implement the model presented. There is no waterproof test, but as much as possible has been done to eliminate this possibility as has been presented. Another option is an error of Popescu et al. in writing down their findings. As the formulas presented are confirmed by other models of electronic transport properties of semiconductors this is unlikely. The possibility of misrepresentation of parameters was investigated by tuning parameters in order to find a better match. Of course one has to keep in mind the physical meaning of these parameters while tuning them. As the behaviour shown is metallic, further research should be done to verify, and where necessary adapt, all parameters. A third possibility is the incompleteness of the model presented. Of course there is no way in checking this, but to ask the writers. In comparison to other models, the model of Popescu et al. seemed the least complicated, while it seemed to gather all important aspects. Hence this model was chosen to be replicated.

For further research I would suggest to take a slightly different model from literature and try to replicate it. Once that succeeds, one can fill in the parameters of lead telluride used in the model presented here and see with which data from Figure 6 it matches. When the step of verification has been completed, all possible materials fulfilling the criteria of the model can be tested to find a good thermoelectric material.

7 Acknowledgements

I would like to thank Bernard Geurts for confronting me with this subject and his help during the assignment. Also the help of Mark Huijben is greatly acknowledged.

Appendices

A Matlab code

In this appendix all Matlab code is given. It consist of several functions, which cover the model described in this paper.

A.1 Model.m

```
1 Start = 50;
2 Step = 10;
3 End = 300;
4
5 a = Start:Step:End;
6 sigma = zeros(1,length(a));
7 S = zeros(1,length(a));
8 kappa = zeros(1,length(a));
9
10 for temp = Start:Step:End;
11     [sigma((temp+Step-Start)/Step),S((temp+Step-Start)/Step),
         kappa((temp+Step-Start)/Step)] = PbTe(temp, 6.1*10^24,
         0.16, 8160, 1730, 10, 0.0072, 0.19, 0.0004, 60*10^-3,
         300*10^-9, 50*10^-9, 10^-4);
12 end
13
14 tpop = 20:20:300;
15 exppopsigma = [800, 600, 400, 400, 700, 1000, 1700, 2800, 4500,
       6500, 9000, 12300, 16400, 17900, 19700];
16 theorypopsigma = [1100, 1000, 1000, 1000, 1300, 1800, 2500,
       3600, 5000, 6800, 9000, 11200, 13800, 16300, 18700];
17
18 exppopS = 10^-6 * [15.5, 25.9, 32.8, 44.8, 62, 82.8, 100,
       113.8, 129.3, 141.4, 155.2, 168.9, 182.7, 196.6, 210.3];
19 theorypopS = 10^-6 * [10.3, 25.9, 37.9, 50, 63.8, 81, 100,
       113.8, 131, 144.8, 155.2, 163.8, 170.7, 177.6, 181];
20
```

```
21 hold on %plot sigma vs T
22 scatter(tpop,exppopsigma)
23 plot(tpop,theorypopsigma)
24 plot(a,sigma,'r')
25 ylabel('\sigma (\Omega m)^{-1}')
26 xlabel('T (K)')
27 hold off
28
29 hold on % plot S vs T
30 scatter(tpop,exppopS)
31 plot(tpop,theorypopS)
32 plot(a,S,'r')
33 ylabel('S (V/K)')
34 xlabel('T (K)')
35 hold off
```

A.2 PbTe.m

```
1 function [sigma,S,kappa] = PbTe(T,p,meffr,rho,vL,D,epsr,Eg0,
    gamma,Eb,L,w,tol)
2 format long
3
4 [Emax1,Emax2,Emax3,mu] = Emaxalt(T,p,meffr,rho,vL,D,epsr,Eg0,
    gamma,Eb,L,w);
5
6 kb = 8.617343*10^-5; %Bolzmann constant (eV/K)
7 m0 = 9.10938291*10^-31; %Mass electron (kg)
8 meff = meffr*m0; %Effective mass (kg)
9 e=1.60217657*10^-19; %Elementary charge (C)
10 Eg = Eg0+gamma.*T; %Bandgap (eV)
11 h=4.135667516*10^-15; %Planck (eV*s)
12 hbar = h/(2*pi);
13
14 int1 = integral(@(E) -E.*scattering1(E,T,rho,vL,D,meffr,epsr,
     Eg0,gamma,Eb,L,w,p).*dofs(E,T,meffr,Eg0,gamma).*difffermi(E,
     mu,T),0,Eb) + integral(@(E) -E.*scattering2(E,T,rho,vL,D,
     meffr,epsr,Eg0,gamma,Eb,L,w,p).*dofs(E,T,meffr,Eg0,gamma).*
```

```
      difffermi(E,mu,T),Eb,10*Emax1,'AbsTol',tol);
15 int2 = integral(@(E) -E.^2.*scattering1(E,T,rho,vL,D,meffr,epsr
      ,Eg0,gamma,Eb,L,w,p).*dofs(E,T,meffr,Eg0,gamma).*difffermi(E
      ,mu,T),0,Eb) + integral(@(E) -E.^2.*scattering2(E,T,rho,vL,D
      ,meffr,epsr,Eg0,gamma,Eb,L,w,p).*dofs(E,T,meffr,Eg0,gamma).*
      difffermi(E,mu,T),Eb,10*Emax2,'AbsTol',tol);
16 int3 = integral(@(E) -E.^3.*scattering1(E,T,rho,vL,D,meffr,epsr
      ,Eg0,gamma,Eb,L,w,p).*dofs(E,T,meffr,Eg0,gamma).*difffermi(E
      ,mu,T),0,Eb) + integral(@(E) -E.^3.*scattering2(E,T,rho,vL,D
      ,meffr,epsr,Eg0,gamma,Eb,L,w,p).*dofs(E,T,meffr,Eg0,gamma).*
      difffermi(E,mu,T),Eb,10*Emax3,'AbsTol',tol);
17
18 sigma = 2*e^2/(3*meff)*int1; %Electrical conductivity (1/ohm m)
19 S = 1/T * (int2/int1 - mu); %Seeback (V/K)
20 kappa = 2*e^2/(3*meff*T) * (int3 - int2^2/int1); %Thermal
      conductivity (W/mK)
21 end
```

A.3 Emaxalt.m

```
1 function [Emax1,Emax2,Emax3,mu] = Emaxalt(T,p,meffr,rho,vL,D,
     epsr,Eg0,gamma,Eb,L,w)
2 format long
3
4 Estep=0.001;
5 Energy = 0:Estep:5;
6
7 kb = 8.617343*10^-5; %Bolzmann constant (eV/K)
8 m0 = 9.10938291*10^-31; %Mass electron (kg)
9 meff = meffr*m0; %Effective mass (kg)
10 h=4.135667516*10^-15; %Planck (eV*s)
11 e=1.60217657*10^-19; %Elementary charge (C)
12
13 mu0 = 0:0.00001:0.1;
14 n = zeros(1,length(mu0));
15 for k = 1:length(mu0)
16     mu1 = mu0(k);
```

```
17      n(k) = 4/sqrt(pi)* (2*pi*meff*kb.*T./(e*h^2))^(3/2) .*
            integral(@(xi) sqrt(xi).*fermidirac(xi.*kb.*T,mu1,T),0,
            Inf,'AbsTol',10^-11);
18 end
19 zoek = find(n>p,1,'first');
20 plot(mu0,n)
21 mu = mu0(zoek);
22
23 df0 = difffermi(Energy,mu,T);
24 g = dofs(Energy,T,meffr,Eg0,gamma);
25 tau = scattering2(Energy,T,rho,vL,D,meffr,epsr,Eg0,gamma,Eb,L,w
     ,p);
26
27 integrand1 = double(-tau.*g.*Energy.*df0);
28 integrand2 = double(-tau.*g.*Energy.^2.*df0);
29 integrand3 = double(-tau.*g.*Energy.^3.*df0);
30
31 [a1,a2] = max(integrand1);
32 [b1,b2] = max(integrand2);
33 [c1,c2] = max(integrand3);
34
35 Emax1 = a2*Estep;
36 Emax2 = b2*Estep;
37 Emax3 = c2*Estep;
38 end
```

A.4 Fermidirac.m

```
1 function f0 = fermidirac( E,mu,T )
2 kb = 8.617343*10^-5; %Bolzmann constant (eV/K)
3 f0 = 1./(exp((E-mu)./(kb.*T))+1);
4 end
```

A.5 Difffermi.m

```
1 function df0 = difffermi( E,mu,T )
2 kb = 8.617343*10^-5; %Bolzmann constant (eV/K)
```

```
3 df0 = -exp((E-mu)./(kb.*T))./(kb.*T.*(exp((E-mu)./(kb*T))+1)
      .^2);
4 end
```

A.6 Scattering1.m

```
1 function [tau1] = scattering1(E,T,rho,vL,D,meffr,epsr,Eg0,gamma
      ,Eb,L,w,p)
2
3 kb = 8.617343*10^-5; %Bolzmann constant (eV/K)
4 m0 = 9.10938291*10^-31; %Mass electron (kg)
5 meff = meffr*m0; %Effective mass (kg)
6 h=4.135667516*10^-15; %Planck (eV*s)
7 hbar = h/(2*pi);
8 Eg = Eg0+gamma.*T; %Bandgap (eV)
9 %epsinf = High frequency dielectric constant
10 %eps0 = Static dielectric constant
11 epsilon = epsr*Eg; %1/epsinf - 1/eps0 (kgm3A-2s-4)
12 eps = 1000; %Dielectric constant
13 e=1.60217657*10^-19; %Elementary charge (C)
14 Z = 2;
15 Ni = 0.5*p;
16 rm = 10^-9;
17
18 C1 = e^(1/2)*h^4/(8*pi^3) * rho*vL^2./(kb.*T) .* 1/((2*meff)
      ^(3/2)*D^2);
19 tau_a = C1 .* E.^(-1/2);
20
21 C2 = h^2/(sqrt(2*meff)*e^(1/2)*kb.*T.*epsilon);
22 tau_o = C2 .* E.^(1/2);
23
24 Em = Z*e^2 / (4*pi*eps*rm);
25 C3 = (Z^2*e^4*Ni/(16*pi*sqrt(2*meff)*eps^2).*log(1+(2.*E./Em)
      .^2)).^(-1);
26 tau_i = C3 .* E.^(3/2);
27
```

```
28 tau_b1 = L*sqrt(e*meff./(2.*E)).*(1+ (4.*E./Eb .* (1-E./Eb))./(
      sinh(sqrt( (2*e*meff*Eb*w^2)/(hbar^2).*(1-E./Eb) )).^2)); %
      When E < Eb
29 tau1 = 1./(1./tau_a+1./tau_o+1./tau_b1+1./tau_i);
30 end
```

A.7 Scattering2.m

```
1 function [tau2] = scattering2(E,T,rho,vL,D,meffr,epsr,Eg0,gamma
      ,Eb,L,w,p)
2
3 kb = 8.617343*10^-5; %Bolzmann constant (eV/K)
4 m0 = 9.10938291*10^-31; %Mass electron (kg)
5 meff = meffr*m0; %Effective mass (kg)
6 h=4.135667516*10^-15; %Planck (eV*s)
7 hbar = h/(2*pi);
8 Eg = Eg0+gamma.*T; %Bandgap (eV)
9 %epsinf = High frequency dielectric constant
10 %eps0 = Static dielectric constant
11 epsilon = epsr*Eg; %1/epsinf - 1/eps0 (kgm3A-2s-4)
12 eps = 1000; %Dielectric constant
13 e=1.60217657*10^-19; %Elementary charge (C)
14 Z = 2;
15 Ni = 0.5*p;
16 rm = 10^-9;
17
18 C1 = e^(1/2)*h^4/(8*pi^3) * rho*vL^2./(kb.*T) .* 1/((2*meff)
      ^(3/2)*D^2);
19 tau_a = C1 .* E.^(-1/2);
20
21 C2 = h^2/(sqrt(2*meff)*e^(1/2)*kb.*T.*epsilon);
22 tau_o = C2 .* E.^(1/2);
23
24 Em = Z*e^2 / (4*pi*eps*rm);
25 C3 = (Z^2*e^4*Ni/(16*pi*sqrt(2*meff)*eps^2).*log(1+(2.*E./Em)
      .^2)).^(-1);
26 tau_i = C3 .* E.^(3/2);
```

```
27
28 tau_b2 = L*sqrt(e*meff./(2.*E)).*(1+ (4.*E./Eb .* (E./Eb-1))./(
       sin(sqrt( (2*e*meff*Eb*w^2)/(hbar^2).*(E./Eb-1) )).^2)); %
       When E > Eb
29 tau2 = 1./(1./tau_a+1./tau_o+1./tau_b2+1./tau_i);
30 end
```

A.8 Dofs.m

```
1 function g = dofs(E,T,meffr,Eg0,gamma)
2
3 m0 = 9.10938291*10^-31; %Mass electron (kg)
4 meff = meffr*m0; %Effective mass (kg)
5 h=4.135667516*10^-15; %Planck (eV*s)
6 hbar = h/(2*pi);
7 Eg = Eg0+gamma.*T; %Bandgap (eV)
8 e=1.60217657*10^-19; %Elementary charge (C)
9 C1 = e^(-3/2)*sqrt(2)/(pi^2)*(meff/(hbar^2))^(3/2);
10
11 g = C1 * sqrt(E.*(1+E./Eg)).*(1+2.*E./Eg);
12 end
```

References

[1] California Institute of Technology. The science of thermoelectric materials, 2014. http://www.thermoelectrics.caltech.edu/thermoelectrics/index.html.

[2] A. Popescu, L.M. Woods, J. Martin, and G.S. Nolas. Model of transport properties of thermoelectric nanocomposite materials. *Physics Review B*, 2009.

[3] Z.H. Dughaish. Lead telluride as a thermoelectric material for thermoelectric power generation. *Physics Review B*, 2002.

[4] Tursky. Semiconductor doping, August 2012. http://www.powerguru.org/semiconductor-doping/.

[5] T.M. Tritt. *Thermal Conductivity Theory, Properties, and Applications.* Kluwer Academic/Plenum Publishers, 2004.

[6] D.M. Rowe and C.M. Bhandari. *Modern Thermoelectrics.* Holt Saunders, 1983.

[7] N. Zettili. *Quantum Mechanics: Concepts and Applications.* Wiley, 2001.

[8] L. Corbijn van Willenswaard. Models for the electronic transport properties of thermoelectric materials. Bachelor Assignment at the University of Twente, 2013.

[9] L.G. Ferreira. Deformation potentials of lead telluride. *Physical Review*, 1965.